Materials Today Bio 26 (2024) 101065

Contents lists available at ScienceDirect

Materials Today Bio

journal homepage: www.journals.elsevier.com/materials-today-bio

Insights into spheroids formation in cellulose nanofibrils and Matrigel hydrogels using AFM-based techniques

Roberta Teixeira Polez [a,b,1], Ngoc Huynh [a,1], Chris S. Pridgeon [a,b], Juan José Valle-Delgado [a], Riina Harjumäki [b,**], Monika Österberg [a,*]

[a] Department of Bioproducts and Biosystems, School of Chemical Engineering, Aalto University, FI-00076, Aalto, Finland
[b] Drug Research Program, Division of Pharmaceutical Biosciences, Faculty of Pharmacy, University of Helsinki, 00790, Helsinki, Finland

ARTICLE INFO

Keywords:
Cellulose nanofibrils
Matrigel
Spheroid formation
Cell interactions
Atomic force microscopy
Cell adhesion molecules

ABSTRACT

The recent FDA decision to eliminate animal testing requirements emphasises the role of cell models, such as spheroids, as regulatory test alternatives for investigations of cellular behaviour, drug responses, and disease modelling. The influence of environment on spheroid formation are incompletely understood, leading to uncertainty in matrix selection for scaffold-based 3D culture. This study uses atomic force microscopy-based techniques to quantify cell adhesion to Matrigel and cellulose nanofibrils (CNF), and cell-cell adhesion forces, and their role in spheroid formation of hepatocellular carcinoma (HepG2) and induced pluripotent stem cells (iPS (IMR90)-4). Results showed different cell behaviour in CNF and Matrigel cultures. Both cell lines formed compact spheroids in CNF but loose cell aggregates in Matrigel. Interestingly, the type of cell adhesion protein, and not the bond strength, appeared to be a key factor in the formation of compact spheroids. The gene expression of E- and N-cadherins, proteins on cell membrane responsible for cell-cell interactions, was increased in CNF culture, leading to formation of compact spheroids while Matrigel culture induced integrin-laminin binding and down-regulated E-cadherin expression, resulting in looser cell aggregates. These findings enhance our understanding of cell-biomaterial interactions in 3D cultures and offer insights for improved 3D cell models, culture biomaterials, and applications in drug research.

1. Introduction

Monolayer cell culture is a useful *in vitro* testing platform to monitor biological events and drug development. However, two-dimensional (2D) culture systems incompletely reflect the intricate physicochemical cellular microenvironment of tissues. *In vivo*, cells exist in a three-dimensional (3D) microenvironment with cell–cell and cell–matrix interactions and complex nutrient transport dynamics [1]. 3D cell cultures, including spheroids, have more *in vivo*-like cellular functions compared to monolayer cultures [2,3]. Additionally, *in vivo* therapeutic effects of spheroids are superior to single-cell transplantation due, in part, to their improved survival and engraftment capacities in harsh conditions [4]. Since the FDA no longer requires animal testing in the development of new drugs and products, the role of cell models has received increased focus [5,6]. Non-animal approaches (e.g., spheroids and organoids) now have the potential to replace, reduce, and refine animal testing.

Spheroids can be produced through matrix-free and matrix-based cell cultures. In matrix-free approaches, cells aggregate freely without supporting structures, using techniques such as low-attachment microplates, or hanging drops. In contrast, matrix-based cell cultures provide support to cells in three dimensions with a matrix. A wide range of biomaterials, such as animal-derived proteins or animal-free hydrogels, can be used as matrices. Biomaterial-based spheroid cultures have been studied extensively for *in vitro* drug toxicity testing and disease modelling [7]. Biomaterials including fibres and proteins offer protection in harsh environments and improve spheroid survival *in vivo* [8]. Furthermore, biomaterials can mimic the natural cell environment e.g., stiffness, further improving the physiological relevance of these models.

Matrigel is an animal-based basement membrane extract derived from murine Engelbreth-Holm-Swarm sarcoma cells. It is widely used as a matrix in 3D culture for a range of cell types. It is a complex and

* Corresponding author.
** Corresponding author.
E-mail addresses: riina.harjumaki@helsinki.fi (R. Harjumäki), monika.osterberg@aalto.fi (M. Österberg).
[1] These authors contributed equally to this work.

https://doi.org/10.1016/j.mtbio.2024.101065
Received 11 November 2023; Received in revised form 30 March 2024; Accepted 15 April 2024
Available online 17 April 2024

variable protein mixture which contains approximately 60 % laminins, 30 % collagens and 8 % entactin [9]. It also contains heparan sulphate proteoglycan (perlecan), TGF-β, epidermal growth factor, insulin-like growth factor, fibroblast growth factor, tissue plasminogen activator, and other growth factors which occur naturally in the EHS tumour. For stem cell culture, it is commonly used as an attachment substrate to provide cell adhesion sites. Compared to synthetic matrixes, Matrigel provides a more physiologically relevant microenvironment. However, due to its animal origin, there is a batch-to-batch variation that can hinder reproducibility [10,11].

Cellulose nanofibrils (CNF, also called nanofibrillated cellulose, NFC) are a biocompatible biomaterial with low toxicity, renewable biomass origin, and have the appropriate mechanical stiffness to mimic extracellular matrix in biomedical uses. The chemical and physical properties of CNF can be tuned for specific biomedical applications. CNF offers improved reproducibility compared to human or animal biomaterials, and increased biosecurity by minimising the possibility of disease transmission. CNF and its derivatives have been used in various biomedical applications [12–18], and have been commercialised for *in vitro* and *in vivo* applications, e.g., GrowDex, FibDex or CELLINK Bioink.

We hypothesize that spheroid formation is the result of the balance between cell–biomaterial interactions and cell–cell interactions. However, due to their complexity, the interactions between the cell and extracellular matrix (ECM) are poorly understood. Recent studies suggest that spheroid formation is possible if cell-cell adhesion forces exceed the intensity of cell-biomaterial adhesion [19,20] but experimental evidence is still lacking. Strong, specific binding interactions between cells and biomaterials may override cell-cell adhesive interactions and disrupt spheroid morphology [21]. Conversely, biomaterials like CNF interact non-specifically with cells which may favour spheroid formation [22–24]. Quantitative measurements of cell interactions are needed to verify these hypotheses. Interactions between cells and biomaterials on the molecular level can influence cell attachment and alter proliferation and migration. Yet, it is not fully understood how biomaterial properties affect the interactions with cells as quantitative measurements of the interactions between cells and different biomaterials are scarce [25].

Quantifying cell interactions with different materials may elucidate the forces that dominate spheroid formation and offer insights into the underlying mechanisms, which can aid the design of novel biomaterials. Thus, to better understand cell adhesion to different biomaterials and cell self-interactions, we combined quantitative surface force spectroscopy data obtained using atomic force microscopy (AFM) with cell culture studies. Cell adhesion was investigated with both single-cell force spectroscopy (SCFS) and colloidal probe microscopy (CPM) techniques using two cell lines, hepatocellular carcinoma (HepG2) and induced pluripotent stem cells (iPS(IMR90)-4). Two different biomaterials were used, basement membrane extract (Matrigel) and cellulose nanofibrils (GrowDex). By establishing a correlation between spheroid formation and cell interactions, these data have the potential to facilitate the identification of new and more suitable materials for 3D cell culture.

2. Materials and methods

2.1. Cell culture and maintenance

HepG2 cells (HB-8065) were purchased from ATCC (Manassas VI, USA) and iPS(IMR90)-4 cells were purchased from WiCell Research Institute (Madison WI, USA). In all experiments, HepG2 cells were cultured in RPMI 1640 (Thermo Fisher Scientific, USA) supplemented with 10 % (v/v) fetal bovine serum (FBS, RPMI, Thermo Fisher Scientific, USA). iPS(IMR90)-4 were cultured in Essential 8 medium (E8, Thermo Fisher Scientific, USA). Henceforth, these will be referred to as culture medium. Cells were cultured under standard tissue culture conditions (37 °C, 5 % CO_2, 95 % relative humidity).

2.1.1. HepG2 maintenance

For HepG2 cells, the medium was changed every three days and cells were passaged at approximately 80 % confluency. The culture medium was initially aspirated, and the cells were washed with 1 x Phosphate Buffered Saline without calcium or magnesium (PBS-, Thermo Fisher Scientific, USA). TrypLE (Thermo Fisher Scientific, USA) was then added, and the cells were incubated at 37 °C for approximately 3–8 min until detachment was observed. Cells were washed from the culture surface with culture medium and centrifuged at 120×*g* for 5 min. The supernatant was discarded, and the pellet was resuspended in culture medium. Finally, the resuspended cells were added to new culture vessels in a 1:4 to 1:5 ratio and returned to the incubator. The cells were allowed to stabilise for at least two days after splitting before AFM measurements.

2.1.2. iPS(IMR90)-4 maintenance

iPS(IMR90)-4 cells were cultured under standard tissue culture conditions in culture medium and on Growth factor reduced (GFR)-Matrigel-coated plates (Corning, Bedford MA, USA). For Matrigel coating, a 1:100 solution of GFR-Matrigel was prepared in DMEM/F12 medium (Thermo Fisher Scientific, USA), approximately 100 μL of diluted Matrigel solution was added per cm^2 of culture surface and allowed to gel at room temperature for 1 h, after which the solution was removed and replaced with culture medium immediately before use. The culture medium was changed daily, and cells were passaged every 2–4 days or at approximately 80 % confluency. For passage, the culture medium was aspirated, and the cells were washed with 1 x PBS-. 0.5 mM EDTA was then added, and the cells were incubated at 37 °C for approximately 3 min until detachment was observed whereupon EDTA was removed. Cells were washed from the culture surface with culture medium, added to new Matrigel-coated culture vessels in a 1:4 to 1:6 ratio, and returned to the incubator. The cells were allowed to stabilise for at least two days after splitting before AFM measurements.

2.1.3. Spheroid formation experiments

3D spheroid formation experiments were carried out in low adhesion round-bottom 96-well suspension plates (Greiner Bio One, Austria). Embedded cultures were further divided into well plates using either Matrigel or CNF.

For CNF embedding, 2.5×10^4 HepG2 or iPS(IMR90)-4 cells per well were prepared in culture medium and mixed with CNF. Culture medium was added to bring CNF final concentration to 0.5 % (w/v). Once prepared, 100 μL of the cell suspension-CNF mixture was added to each well of a 96-well suspension plate and incubated at 37 °C for 10 min before a further 100 μL of culture medium was gently added on top.

For Matrigel embedding, a suspension of 2.5×10^4 cells per well in culture medium was prepared and mixed with an equal volume of cold Matrigel. Next, 100 μL of the cell-Matrigel mixture was added to each well of a flat-bottomed, 96-well suspension culture plate, avoiding bubble formation. The Matrigel was allowed to gel at 37 °C for 10 min before an additional 100 μL of culture medium was added.

In all conditions, culture medium was changed with the frequency previously described for each cell line. After 72 h, cells were imaged using a Leica DMIL LED brightfield microscope with a Leica EC4 camera (Leica Microsystems, Heerbrugg, Switzerland). After 7 days, viability was determined using an AlamarBlue viability assay.

2.2. Cell viability and metabolic activity assay

AlamarBlue Cell Viability Reagent (Thermo Fisher Scientific, USA) was used to determine the metabolic activity according to the manufacturer's protocol. The protocol was conducted in darkness. Briefly, the medium was replaced with a solution of 10 % (v/v) AlamarBlue reagent and culture medium and incubated for 24 h. After incubation, the AlamarBlue solution was collected and centrifuged at 200×*g* to remove particulates. The supernatant was transferred into a 96-well plate and

the fluorescence (530 nm excitation, 590 nm emission) was determined using a Varioskan LUX Multimode Microplate Reader (Thermo Fisher Scientific, USA).

Viability was assessed by LIVE/DEAD staining (Thermo Fisher Scientific, USA). Viable cells were stained with calcein AM (495 nm excitation, 515 nm emission) and dead cells were stained with ethidium homodimer-1 (530 nm excitation, 620 nm emission). Thirty minutes prior to imaging, the culture medium of cells was replaced with medium containing a final concentration of 4 μM calcein AM and 8 μM ethidium homodimer-1, for HepG2 cells, fetal bovine serum was excluded in the refreshed medium. Samples were visualised using an Aurox Clarity spinning-disc confocal device (Aurox Ltd, United Kingdom) coupled to an Axio Observer Z1 microscope (Zeiss, Germany) with CO_2 and temperature control (The Cube & The Box, Life Imaging Services, Switzerland). Image processing and z-projections were performed using Fiji [26].

2.3. Gene expression

Spheroids, cultured as indicated above, were lysed in Qiazol (Qiagen, Germany) at 1, 3, 7 or 10 days of culture and RNA was recovered using a standard phenol-chloroform extraction. Reverse transcription was performed using the High-Capacity RNA-to-cDNA kit (Thermo Fisher Scientific, USA) according to the manufacturer's protocol. Quantitative real-time polymerase chain reaction (qRT-PCR) was performed using TaqMan chemistry. The experimental genes were ALB, PCNA and NANOG, for which the control gene was ACTB, and CDH1, CDH2 and ITGA5, for which the control gene was TBP (all Thermo Fisher Scientific, USA). Reactions were performed using a StepOnePlus Real-Time PCR instrument (Thermo Fisher Scientific, USA).

2.4. Preparation of probes for force measurements

Tipless cantilevers (HQ:CSC38/tipless/Cr–Au, MikroMasch, Wetzlar, Germany) with spring constants ranging from 0.05 to 0.30 N/m were used. Cantilevers' parameters (length and width) were measured with a Leica DM750 microscope (Leica Microsystems, Heerbrugg, Switzerland) with LAS software. Cantilevers were further cleaned with oxygen plasma treatment (Pico Surface Plasma Cleaner, Diener Electronics, Germany) at 250 mTorr for 5 min to remove organic contaminants and maximise the number of surface –OH groups.

For force measurements using the colloidal probe technique, glass microparticles (Polysciences, Warrington PA, USA) were attached to the tipless cantilevers and cleaned with piranha solution (3:1 mixture of H_2SO_4 and H_2O_2). A motorised PatchStar micromanipulator (Scientifica, Uckfield, UK) and an optical adhesive #81 (Norland Products, Cranbury NJ, USA) were used for attaching the microparticles (Ø ~ 30 μm) on the cantilevers. Briefly, a sharp wire was used to put glue on a tipless cantilever, then a single particle was picked up with another sharp wire and placed on the glue. The probes were cured for 15 min under UV light at 365 nm (UV Crosslinker CL-508, UVITEC, Cambridge, UK). The probe radius was measured with a Leica DM750 microscope (Leica Microsystems, Heerbrugg, Switzerland) with LAS software and the radius ranged from 7 to 20 μm. The custom probes were further cleaned with 30 min of UV ozone radiation exposure (UV Ozone ProCleaner, BioForce Nanoscience Inc., Ames IA, USA) before coating with CNF or Matrigel.

The probes were coated with the biomaterials via adsorption as previously reported [27]. Matrigel (Corning Corp., Bedford MA, USA) was coated on glass microparticles by adsorption for 30 min and rinsed with Dulbecco's phosphate-buffered saline with calcium and magnesium (1× DPBS+, Gibco, USA). CNF dispersion was prepared using GrowDex (UPM Biomedicals, Helsinki, Finland) as reported elsewhere [28]. The CNF hydrogel (1.5 wt%) was diluted in Milli-Q water and ultrasonicated at 25 % amplitude for 5 min with a Branson sonifier S-450 D (Branson Corp., Danbury CT, USA). The dispersion was then centrifuged at 8000×*g* for 30 min at room temperature using an Eppendorf centrifuge 5804R (Eppendorf, Hamburg, Germany) to separate the supernatant fraction with the finest cellulose fibrils for use in the experiments (0.25 % dry matter content). The fine CNF dispersion was coated on glass microparticles by firstly adsorbing PEI 2.5 mg mL^{-1} (polyethyleneimine) for 10 min, rinsing with milli-Q water and drying under nitrogen. Then, CNF dispersion was adsorbed for 10 min, the probes were rinsed with milli-Q water and dried under nitrogen. The same coating protocols were used to coat flat substrates for single-cell force spectroscopy experiments.

To prepare the cantilever for single-cell measurements, tipless cantilevers were chemically functionalized for a single suspended cell to be attached. They were coated with Cell-Tak Cell and Tissue adhesive (Corning Corp., Bedford MA, USA) by adsorption for 30 min. After coating they were rinsed with 1 x DPBS+ (Gibco, USA) and stored at 2–8 °C before attachment of cells and use in experiments. The Cell-Tak was diluted in sodium bicarbonate 0.1 M and sodium hydroxide 0.1 M in a ratio of 57:2:1 as recommended by the manufacturer. For cell attachment, a single suspended cell was visually identified under a microscope. The functionalized cantilever's tip was meticulously positioned over the cell and gently brought into contact with the single cell for a duration of 10–20 s [29]. Upon retracting the cantilever, the cell was no longer visible on the surface but was securely attached to the cantilever. Microscopy images of the cells attached to cantilevers were acquired using an inverted optical fluorescence microscope (Fig. S1) (Olympus IX 73, Olympus Corporation, Japan) and cell radius was determined using Fiji ImageJ software [30] (NIH, Bethesda, Maryland, USA). The radii of the cells ranged from 7 to 10 μm for both HepG2 and iPS(IMR90)-4 cells.

2.5. High-resolution images of biomaterial coating

High-resolution images of CNF coating were recorded on a MultiMode 8 AFM with a NanoScope V controller and an E scanner (Bruker, Santa Barbara CA, USA) in dry conditions using ScanAsyst mode and ScanAsyst-Air probes (Bruker). For Matrigel coating, high-resolution images were recorded using a NanoWizard IV XP BioScience AFM (JPK-Bruker, Berlin, Germany) in liquid (1 x DPBS+) using ScanAsyst Fluid + probes.

Microstructure images of the coated probes were acquired with a Zeiss SIGMA VP field emission scanning electron microscope (FESEM) at the beam voltage of 1 kV, using type II secondary electrons (SE2), and reaching a working distance of 5.5 mm and magnification of 1,300×.

2.6. Force measurements

All force spectroscopy measurements were acquired using a NanoWizard IV XP BioScience AFM (JPK- Bruker) with a CellHesion 200 head mounted on top of an inverted optical fluorescence microscope (Olympus IX 73, Olympus Corporation, Japan). The system was located inside an acoustic enclosure and vibration isolation system. Spring constants of the probes were determined using the thermal noise method [31,32] and ranged from 0.05 to 0.30 N/m.

For the colloidal probe microscopy technique (CPM), the cantilever with the attached biomaterial-coated microparticle was approached to a colony of cells on a flat substrate, whereas for single-cell force spectroscopy (SCFS) a single cell attached to a tipless cantilever was approached to a colony of cells or biomaterial-coated flat surfaces. Force measurements were carried out by approaching the cantilever with the attached colloidal probe or cell to the corresponding substrate (cells or biomaterial surfaces) at a constant velocity of 2 μm/s until a maximum force of 8 nN was applied, and after a certain time in contact the cantilever was retracted at the same speed. Forces acting between cell-cell or cell-biomaterial cause the cantilever to deflect. The deflection of the cantilever was monitored and plotted in a graph of deflection *versus* piezo movement. Cells were allowed to rest for 20 s before each measurement started. Typically, 5 to 10 deflection-height curves per cell

were recorded in constant force mode for each contact time (1, 30, and 60 s) on two random locations for each Petri dish to check data reproducibility. The experiments were repeated for each system in at least 3 separate occasions, using a minimum of 5 probes and minimum of 5 Petri dishes. The maximum measurement time was 1 h per Petri dish. All measurements were carried out in DPBS + media at 37 °C using a Petri dish Heater (JPK, Bruker, USA).

The raw force-distance curves consisting of the vertical deflection signal as a function of the z-piezo displacement were converted into force-separation curves using the JPK Data Processing software. The deflection sensitivity and spring constant parameters were obtained during calibration before each measurement. JPK Data Processing software was also used to fit the baseline of the retraction curve. Further data processing was carried out using a custom routine written in Python to determine the adhesion parameters (maximum adhesion force, adhesion energy and rupture length). The adhesion energy was obtained by integrating the area enclosed between the retraction force curve (negative values) and the baseline. The adhesion force was defined as the minimum point on the retraction curve, and the rupture length was calculated as the difference between the two intersections with the curve baseline. For the experiments using the colloidal probe technique, the resulting forces were normalised by the microparticle radius.

2.7. Statistical analysis

Values are expressed as mean ± standard deviation (SD). Statistical analysis was performed using analysis of variance (one-way ANOVA) followed by Fisher's multiple comparison test or Student's t-test. All statistical analyses were carried out using Prism 5 (GraphPad, San Diego CA, USA).

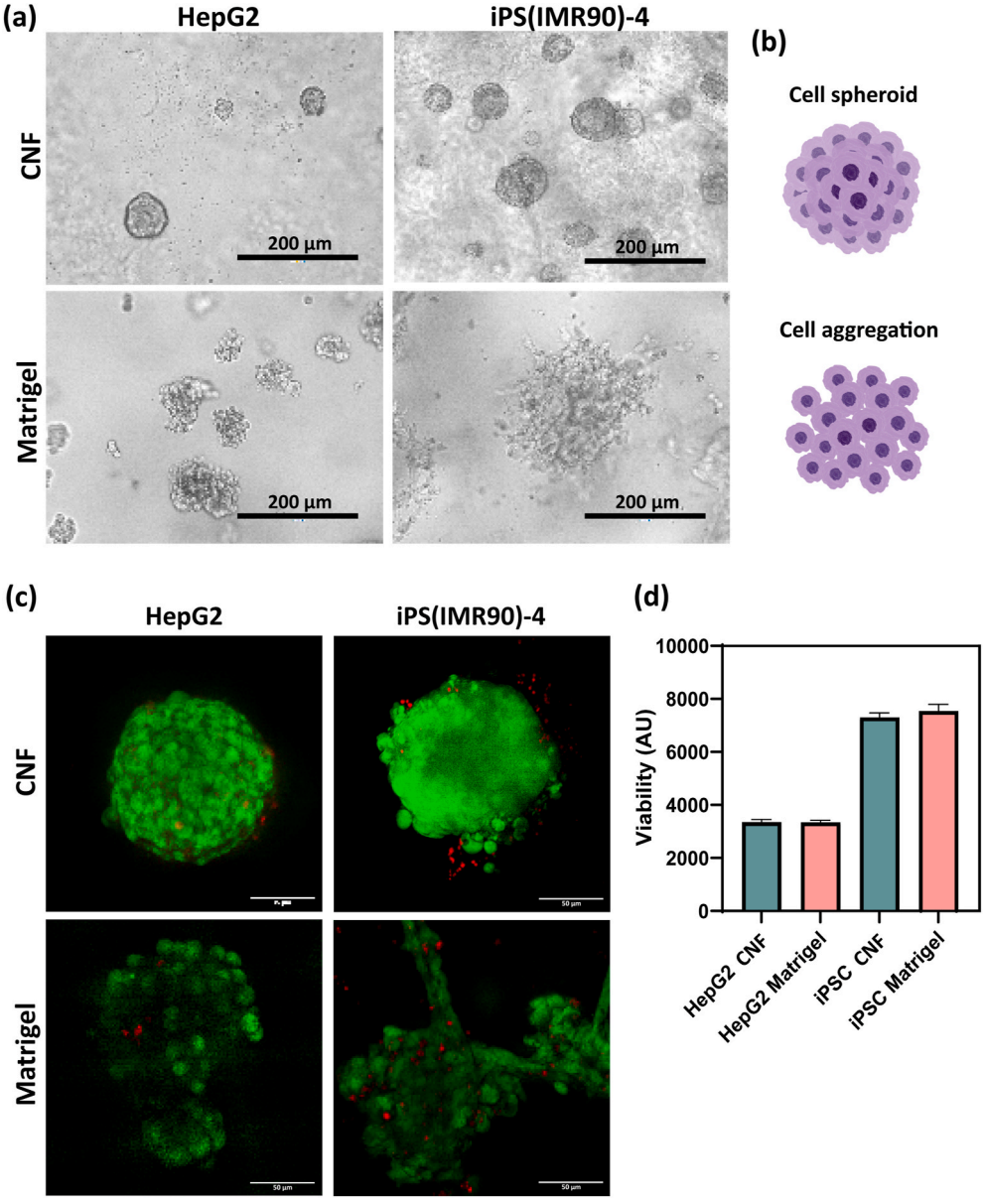

Fig. 1. **(a)** Light microscopy images of HepG2 and iPS(IMR90)-4 spheroids cultured in Matrigel and CNF after 3 days. Scale bar: 200 µm. **(b)** Illustration of spheroid and cell aggregates formed in the 3D cultures. **(c)** LIVE/DEAD confocal z-projections of the spheroids stained with calcein-AM (green) and ethidium homodimer-1 (red). Scale bar: 50 µm. **(d)** Viability of HepG2 and iPS(IMR90)-4 cells after 7 days in Matrigel or CNF-embedded cultures. Results expressed as mean ± SD. (For interpretation of the references to colour in this figure legend, the reader is referred to the Web version of this article.)

3. Results and discussion

3.1. Spheroid cell culture

To study the mechanisms of spheroid formation in CNF and Matrigel, iPS(IMR90)-4 and HepG2 cells were cultured embedded in both hydrogels. Their viability and morphology were observed and later correlated to the interactions recorded by AFM techniques.

Clusters of iPS(IMR90)-4 and HepG2 cells formed in both matrices, although their morphologies differed (Fig. 1a). In CNF, HepG2 cells formed spheroids with rounded but irregular shape and varying diameter (20–100 μm), whereas in Matrigel, they formed large cell aggregates with looser morphology, i.e., individual cells could be recognised in each cluster (Fig. 1a and b). This potentially indicates weaker cell-cell interactions compared to the rounder and denser clusters formed in CNF [33–35]. This observation contrasts with a previous study where HepG2 cells formed large spheroids only in the presence of 2.5 % Matrigel [36].

Similarly, loose clusters were observed in Matrigel for iPS(IMR90)-4. However, when cultured in CNF, iPS(IMR90)-4 formed large, dense, and uniformly structured spheroids, approximately 100 μm in diameter with a distinctive shell-core morphology [36,37]. A comparison of the two cell lines cultured in both matrices showed that iPS(IMR90)-4 spheroids in CNF increased density over time, aligning with findings from previous studies [38,39]. Lin et al. demonstrated that HepG2 spheroids showed a continuous increase in compactness, with the fastest aggregation rate observed in the initial 12 h.

The viscoelastic properties of hydrogels alter cellular behaviour, ideally, the matrix would mimic those of physiological ECM. At 0.5 % concentration, CNF has a shear viscosity of 1500–8000 Pa s, storage modulus (G') of ~10 Pa, and loss modulus (G'') of ~2 Pa at 0.1 Hz and room temperature [22]. Matrigel also exhibits comparable viscoelasticity, with a G' of ~30 Pa and a G'' of ~4 Pa at 37 °C [40]. Importantly, both hydrogels resemble physiological ECM properties, such as decellularized lung tissue (15 Pa) or adipose matrix (10–15 Pa at 4 mg/mL) [41,42].

In addition to viscoelastic properties, hydrogel concentration significantly impacts cell behaviour by influencing matrix stiffness, thereby affecting cellular motility, and proliferation. Previous studies have fine-tuned CNF concentration for specific cell types; for example, HepG2 formed spheroids in 0.8 %, 1.0 %, and 1.7 % CNF hydrogels [18,22,43,44], whereas iPS(IMR90)-4 formed spheroids in 0.55 % and 0.5 % CNF hydrogels [23,20]. Given the variability of Matrigel, maintaining consistent parameters like protein composition or stiffness between batches poses a challenge. Consequently, established conditions, such as 50 % Matrigel (4–5.5 mg/mL protein content) supporting HepG2 spheroid formation [45–47], were adopted and applied to hPSCs, aligning with CNF conditions.

Similar metabolic activity was observed between cells cultured in both CNF and Matrigel (Fig. 1d). Furthermore, LIVE/DEAD staining showed that spheroids remained viable for at least 7 days in culture (Fig. 1*c*). Some dead cells were observed but these were predominantly single cells outside the spheroids. Additionally, there was no difference in the expression of the proliferation marker PCNA (Fig. S2). This suggests that differences in spheroid formation arise from the differences in cell-biomaterial interactions rather due to differences in cell viability or proliferation.

Regarding cellular phenotype, HepG2 spheroids had increased gene expression of albumin, a liver specific marker, when cultured in 3D compared to 2D (Fig. S3*a*). Expression was higher in HepG2 spheroids in CNF than in Matrigel. These findings are consistent with previous reports, where embedding HepaRG cells in CNF improved hepatic phenotype of liver cells, leading to increased expression of albumin [18,22]. In iPS(IMR90)-4 spheroids, the expression of the pluripotent marker NANOG was consistently maintained throughout the experimental duration (Fig. S3*b*). These findings are in agreement with previous reports where similar expression patterns of OCT4 and NANOG were observed in hPSCs cultured in CNF for up to 26 days [23]. Therefore, it may be concluded that the differences in spheroid morphology between matrices is not attributable to altered differentiation in either matrix.

While cell viability is an essential parameter to assess cell health and survival, it is insufficient to fully explain the intricacies of spheroid formation. We hypothesised that spheroid formation depends on the balance between cell–cell and cell–biomaterial interactions. Stronger adhesion between cells than between cells and biomaterials were anticipated to produce spheroid formation [19,20]. However, the correlation between spheroid formation and cell interactions has rarely been explored in previous studies with actual measurements of the binding forces involved. To improve our understanding of the spheroid formation process, highly sensitive AFM-techniques were used to quantify the interaction forces between cells, and between cells and biomaterials.

3.2. Quantifying adhesion forces between cells and biomaterials

Investigating unicellular interactions can help improve our understanding of biological processes as these interactions regulate cell structure and function. In particular, the formation of spheroids or cell aggregates was expected to be dictated by cell interactions with the matrix material and cells. To investigate these forces, CPM and SCFS were used. In CPM, a biomaterial-coated sphere was used as the probe, to quantify cell adhesion to Matrigel and CNF. SCFS, with a single cell attached to a tipless cantilever, was used to measure the adhesion forces between cells.

CPM was effective in analysing cell-biomaterial interactions. The well-defined spherical geometry of the probe allowed comparison between CPM experiments conducted with different colloidal probes by normalising the force measurements with the radius of the corresponding probe. Comparing the cell-biomaterial interactions measured by CPM with the cell-cell interactions quantified by SCFS could help elucidate the mechanisms of spheroid formation and offer insights to improve biomaterial design, optimise culture protocols, and enhance tissue engineering applications.

A uniform coating of Matrigel and CNF is essential to ensure reproducibility of CPM experiments. Therefore, the biomaterial coating on the colloidal probes and the surface morphology of the substrates were characterised with FESEM and AFM (Fig. S4). The surface profile of CNF coating was a fibrillar entangled network with porous structure whereas Matrigel surface presented an irregular structure composed of globular units similar to previous SEM images of Matrigel coatings [48] and AFM images of laminin and collagen IV protein films [24,27,49].

Force-distance curves were obtained for HepG2 and iPS(IMR90)-4 cells interacting with similar cells or with CNF and Matrigel at different contact times ranging from 1 to 60 s. Fig. 2 displays the representative curves and all recorded curves can be found in Fig. S5. To facilitate the comparison with the cell-material normalised forces, the forces between cells were also normalised by the radius of the cell attached on the AFM cantilever, which should be considered as an approximation that may still allow for the identification of adhesion trends. Qualitatively, the force-distance curves for cells showed distinct adhesion behaviour, indicating that the different natures of the biomaterials resulted in different force-curve profiles. For CNF and Matrigel in contact with HepG2 cells, relatively narrow adhesion peaks with a rapid return to zero force were observed, whereas the adhesion peaks between HepG2 cells were more intense, broader and with longer rupture lengths (Fig. 2a). Stem cells exhibited force curve profiles more similar to each other, but also with longer rupture lengths for cell-cell force curves compared to cell-biomaterial ones (Fig. 2b).

By varying the contact time, the temporal development of adhesion forces could be investigated. The adhesion was found to increase with longer contact times, up to 60 s, across all systems studied, in agreement with previous studies [24,50,51]. This observation suggests that a

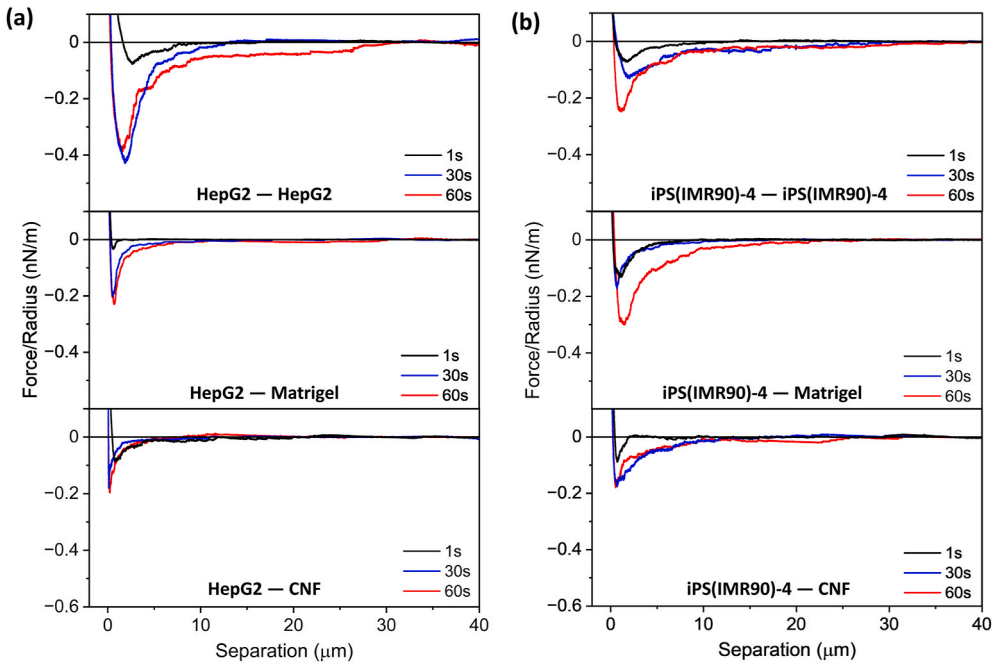

Fig. 2. Representative examples of retraction force-distance curves at different contact times. **(a)** HepG2 — HepG2; HepG2 — Matrigel and HepG2 — CNF interaction. **(b)** iPS(IMR90)-4 — iPS(IMR90)-4, iPS(IMR90)-4 — Matrigel and iPS(IMR90)-4 — CNF.

certain time is needed for the formation of specific ligand-receptor bonds. Longer contact periods could also lead to larger deformation of the cells, resulting in larger contact areas and, consequently, stronger adhesion.

A detailed quantitative analysis of the cell-cell and cell-biomaterial adhesion for 60 s contact time is presented in Fig. 3 and Table 1. The corresponding results for 1 and 30 s are shown in Fig. S6 and Table S1. The values for adhesion energy, maximum adhesion force and rupture length were extracted from the force-distance curves after normalising the force by the probe radius, as is usually done in CPM experiments. The adhesion energy, also called work of adhesion, was calculated by the integration of the retraction curve, and represents the overall adhesion energy of the rupture of formed complexes and a mechanical component due to cell deformation. The maximum adhesion force (also called detachment force or pull-off force) is the lowest point in the curve and depicts the maximum strength of cell-substrate binding. The rupture

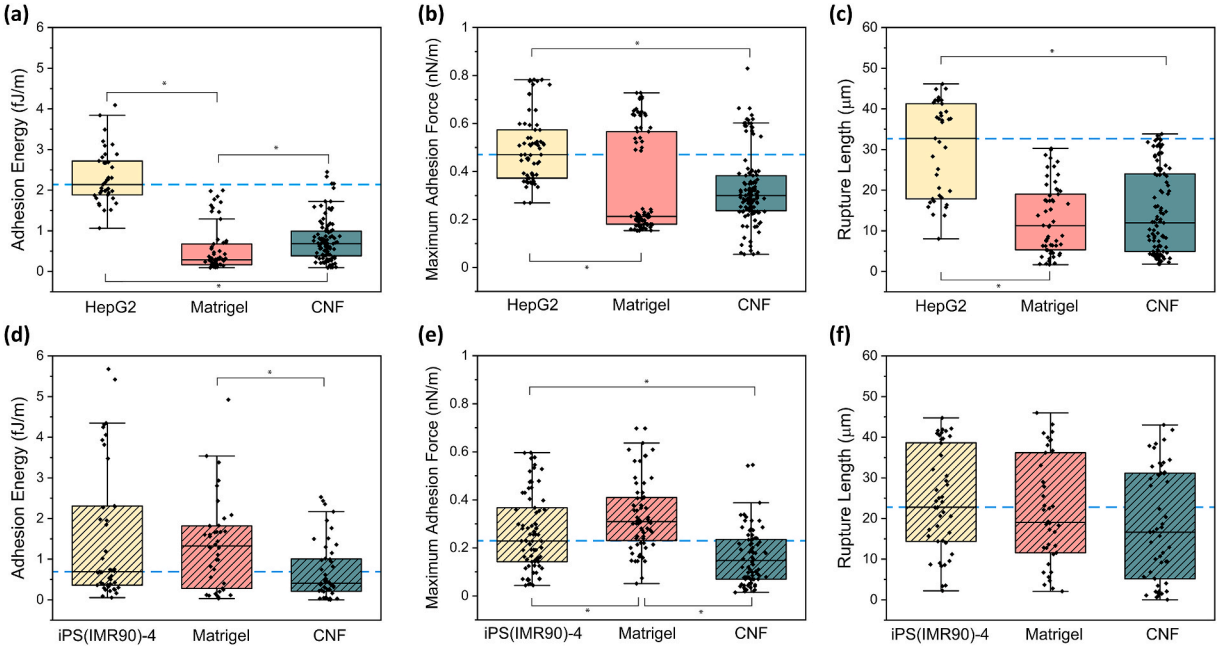

Fig. 3. Box plot of **(a)** adhesion energy, **(b)** maximum adhesion force and **(c)** rupture length for HepG2 interaction with HepG2 cells (yellow boxes), Matrigel (red boxes), and CNF (green boxes) for 60 s contact time; and box plot of **(d)** adhesion energy, **(e)** maximum adhesion force and **(f)** rupture length for iPS(IMR90-4) interaction with iPS(IMR90-4) cells (dashed yellow boxes), Matrigel (dashed red boxes), and CNF (dashed green boxes) after 60s contact time. Results expressed as mean ± SD. Asterisks (*) indicates significant values at the $p \leq 0.05$ determined using a Tukey test. (For interpretation of the references to colour in this figure legend, the reader is referred to the Web version of this article.)

Table 1
Mean values of adhesion energy, maximum adhesion force and rupture length for HepG2 and iPS(IMR90)-4 in contact with Matrigel and CNF for 60s. Cell-biomaterial interactions were measured by CPM.

	Adhesion energy (fJ/m)	Maximum adhesion force (nN/m)	Rupture length (μm)
HepG2 - HepG2	2.13 ± 0.65	0.47 ± 0.13	32.7 ± 11.3
HepG2 - Matrigel	0.29 ± 0.55	0.21 ± 0.19	11.3 ± 8.3
HepG2 - CNF	0.69 ± 0.51	0.29 ± 0.14	11.9 ± 10.1
iPS(IMR90)-4 - iPS (IMR90)-4	0.69 ± 0.94	0.26 ± 0.15	22.8 ± 12.6
iPS(IMR90)-4 - Matrigel	1.33 ± 1.12	0.31 ± 014	19.0 ± 13.2
iPS(IMR90)-4 - CNF	0.41 ± 0.32	0.14 ± 0.11	18.1 ± 13.8

length or length of detachment is the maximum distance that the cells are stretched before they were completely detached from the substrates or from other cells. All cell experiments generally exhibited a broad distribution of data points including some outliers. Quantitative force measurements using living cells still represent a challenging task due to the complexity and variability of biological systems. The high standard deviation observed in all the measured parameters could be explained by the heterogeneity of the cells, as well as by their high sensitivity to slight changes in the environmental conditions, as has also been observed in previous reports on cell adhesion [50,52,53]. Logically, a larger variability in the results was generally obtained when measuring the adhesion between two cells in comparison to the adhesion between a cell and materials [54].

Due to the inherent imprecision of normalising forces to cell radius without accounting for cell deformation in SCFS experiments (Fig. 3 and Table 1), it is important to approach the values of adhesion parameters for cell-cell interaction with caution. Despite this limitation, it seemed evident that HepG2 cells exhibit stronger adhesion to one another than to CNF. This observation aligns with the hypothesis that the formation of HepG2 spheroids in CNF cultures is driven by cell-cell interactions, which dominate over cell-material interactions (Fig. 1a).

However, the comparison of adhesion force and energy between HepG2 cells and Matrigel revealed values that are similar or lower than the corresponding values for CNF, contrary to our initial hypothesis. Stronger adhesion forces of HepG2 cells to Matrigel than to CNF were expected because loose aggregates were formed instead of spheroids in Matrigel cultures (Fig. 1a). However, the force measurements did not support this hypothesis. As expected, the rupture length was larger for the HepG2-HepG2 system since two cells were stretched in the retraction force curves.

On the contrary, the adhesion of stem cells to Matrigel seemed to be stronger than to other stem cells, especially when comparing the values of adhesion energy. This supports the initial hypothesis to explain the lack of well-defined spheroids of iPS(IMR90)-4 cells observed in Matrigel (Fig. 1a). Conversely, iPS(IMR90)-4 cells formed spheroids when embedded in CNF, but the adhesion between iPS(IMR90)-4 cells did not seem to be much stronger than their adhesion to CNF. This challenges the initial hypothesis and suggests that the intensity of adhesion between cells or cell-materials may not be the determining factor for spheroid formation.

To confirm these trends, the interaction of HepG2 cells with Matrigel and CNF was also analysed by SCFS. The different set-up of these experiments, with cells attached to the AFM cantilever and the materials adsorbed on a flat substrate, can test whether the different configuration and polarity of the probed cells affects adhesion (Fig. S7). Additionally, it allows for direct comparison of adhesion energy and maximum adhesion forces without normalisation by probe radius. The force-distance curves and the corresponding adhesion parameters are displayed in Figs. S8 and S9 and Table S2. In general, the same trends in adhesion observed in CPM experiments were also observed in SCFS measurements. Comparing the adhesion energies after 60 s in contact, the adhesion between HepG2 cells was stronger than between HepG2 cells and the tested biomaterials. Furthermore, no clear differences were observed for the adhesion of HepG2 to Matrigel and CNF.

The results from both CPM and SCFS experiments indicate that the overall adhesion of cells to materials is not the determining factor for spheroid formation and cannot explain why HepG2 cells form spheroids in CNF but looser cell aggregates in Matrigel. The adhesion force and energy values result from the sum of several constituent forces, from physical forces such as van der Waals and hydrogen bonds, simple entanglements, or specific binding mediated by cellular adhesion molecules like integrins and cadherins. Therefore, the force curves were examined, and the types of bonds formed between the cells and the materials were identified. The malignant HepG2 cells demonstrated stronger cell-cell adhesion than the comparatively sensitive iPS(IMR90)-4 cells, indicating that these cell lines express different surface adhesion molecules. The expression of different cell receptors could also be the reason for the different adhesion trends observed for stem cells (iPS(IMR90)-4—Matrigel > iPS(IMR90)-4—iPS(IMR90)-4 > iPS(IMR90)-4—CNF) and for HepG2 cells (HepG2—HepG2 > HepG2—CNF > HepG2—Matrigel). Notably, integrin receptors on the cell membranes can specifically bind laminin, a main component of Matrigel absent in CNF [24,51]. Additionally, the different adhesion energy between HepG2—Matrigel and iPS(IMR90)-4—Matrigel may be related to different integrin densities expressed on HepG2 and iPS(IMR90)-4 cell membranes. Therefore, a detailed analysis of the individual binding force events present in the force-distance curves was performed and correlated to the presence or absence of several important cell receptors of HepG2 and iPS(IMR90)-4 cells to better understand the spheroid formation process.

3.3. *Understanding the effect of bond types on spheroid formation*

On the molecular level, cell adhesion is governed by a combination of interactions involving both non-specific and specific interactions, as illustrated in Fig. 4. Non-specific interactions are physicochemical forces such as hydrogen bonds, van der Waals forces, and electrostatic forces that occur between the cellular phospholipid membrane and the substrate. These non-specific interactions do not induce significant changes in the cell membrane and usually rely on their number or density to create a stronger effect. Specific interactions, on the other hand, occur through ligand-receptor binding mediated by cell adhesion molecules like integrins and cadherins. These specific bindings, once established, are usually further reinforced by the recruitment and assembly of intracellular proteins, and together they enable cellular mechanosensing and mechanotransduction [55]. When put under tension as in the retracting motion in AFM techniques, they transfer force throughout the cytoskeletal network and undergo deformation, e.g., stretching or tethering, of both these local adhesion points and of the whole cell.

During specific interaction with proteins or other bioactive substrates, integrins are frequently involved, e.g., as the cellular receptor that binds to ECM proteins such as laminins, fibronectin, and collagens. Specifically, the integrin receptors on cells interact with peptides called cell binding domains, in proteins or bioactive materials. For instance, fibronectin and entactin can interact with α5β1 or αVβ5 integrins through the RGD domain (arginylglycylaspartic acid), while laminins or collagens can interact with for example α6β1 or α2β1 integrins using their own cell binding domains [56–58]. Cadherins, another family of cellular adhesion molecules, are commonly involved in cell-cell adhesion. Cadherins typically share cadherin repeats which bind to form calcium-dependent homodimers as part of adherens junction between cells.

CNF hydrogels are non-toxic and animal-component free. They mimic the viscoelastic properties and fibril structure of natural ECM but lack specific binding domains for cell membrane receptors. Cellulose does not form specific protein interactions with mammalian cells [24,

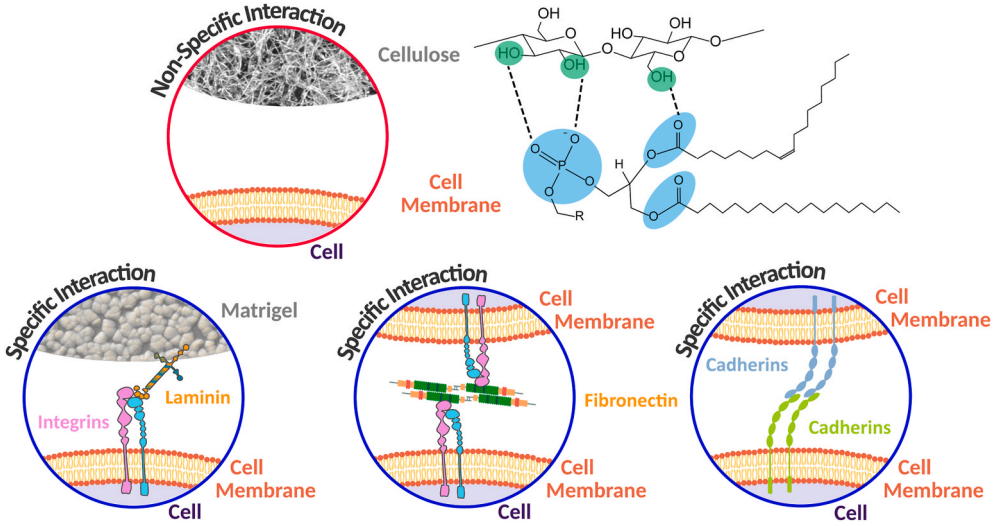

Fig. 4. Schematic illustration of different types of cell interaction. Non-specific interaction between cell-cellulose via hydrogen bonds. Specific interaction: cell-Matrigel interaction via integrin-laminin bond; cell-cell interaction via fibronectin bridge; cell-cell interaction via cadherin-cadherin bond.

59]. Instead, cellulose-cell interactions are predominantly non-specific, relying on electrostatic forces, hydrogen bonds, and van der Waals forces. Indeed, our recent study confirmed that CNF adhesion to WA07 stem cells and HepG2 cells was not mediated by integrins, and it was weaker than the cell adhesion to ECM protein laminin-521 [24,51]. However, adsorbing laminin-521 or poly-L-lysine on CNF substrates enhances cell adhesion [60].

Molecular dynamics simulations showed that cellulose–cell membrane binding is mainly driven by hydrogen bonds between phosphate groups from the phospholipid bilayers and cellulose hydroxyl groups [61]. Similarly, other polysaccharides like carboxymethylcellulose interact with lysine, proline, and threonine in collagen through hydrogen bonds and van der Waals interaction, with high affinity but low energy [62]. Furthermore, the bonding between hyaluronic acid and CD44 cells with adhesion force in the range of 0.06–0.09 nN [63], is comparable to the forces required to unbind a single integrin-ligand bond, which requires 0.005–0.01 nN [64,65], even though hyaluronic acid does not have the specific domains to interact with cell receptors. These observations suggest that cell adhesion depends on the type of bond, the strength of each bond and the number of binding sites between cell and biomaterial surface.

Negative charge density and a highly hydrophilic surface, such as in TEMPO-oxidized CNF, has been reported to limit initial cell attachment, and contribute to quicker and larger spheroid formation [66]. However, research on spheroid formation in TEMPO-oxidized CNF is underexplored, lacking optimized protocols for the cells used in this study. Due to variations in viscoelastic properties among different cellulose hydrogels, extensive optimization would be required before studying the role of matrix charge alone. Future studies may consider studying interactions between different modifications on CNF and explore their effects on spheroid formation.

The interaction between cells and Matrigel is predominantly governed by specific integrin-laminin binding [58] which correlate to the cell aggregates observed in Matrigel. Matrigel primarily consists of laminin (60 %) which interacts with laminin-binding integrin receptors α6β1. Studies have demonstrated that blockade of either subunit α6 or β1 decreases cell binding efficiency [67,68].

While the measurement set-up of CPM allows for direct quantification of cell-substrate interactions, the comparison of adhesion force and energy values alone did not elucidate the manner in which these cell lines interacted with CNF or Matrigel. Therefore, it is difficult to explain the underlying mechanism of spheroid formations in these hydrogel matrices with these data alone.

Spheroid formation occurs over multiple stages. Cells first aggregate into loose clusters by binding to ECM proteins like fibronectin on the peripheral cell surface [39]. During this first stage, the specific interaction between ECM proteins and integrins is particularly important. Fibronectin, for example, assists in the clustering of human dermal fibroblasts [69]. These ECM proteins can be secreted by the cells themselves or provided in the culture medium. When cells are in proximity, they accumulate cadherin-cadherin homophilic bonds to create adherens junction, which tightens loose cell clusters into tightly packed spheroids.

Several studies suggest the importance of E-cadherins, N-cadherins and fibronectin-integrin (mainly α5β1 integrins) in spheroid formation [69,70]. Therefore, we examined the expression of ITGA5, CDH1 and CDH2, encoding integrin subunit α5, E-cadherin and N-cadherin, respectively, for 10 days during the process of spheroid formation (Fig. 5).

In HepG2, ITGA5 expression was approximately 20-fold lower than in iPS(IMR90)-4 at day 0 and declined over time in Matrigel culture. ITGA5 was undetected in CNF-embedded culture for HepG2 but was comparatively high in iPS(IMR90)-4 in both culture conditions and was maintained throughout the experiment. In Matrigel culture, expression peaked at day 10 at approximately 440-fold higher than HepG2 at day 0. In CNF culture ITGA5 expression decreased slightly with time but remained higher than in HepG2 cells by day 10.

ITGA5 encodes integrin subunit α5, part of integrin α5β1 which is implicated in the binding of fibronectin and other RGD-containing ECM proteins. The absence of ITGA5 in HepG2 cells cultured in CNF from day 1 to day 10 could indicate that the production of integrin subunit α5 was ceased already during the first 24 h. Furthermore, the decreasing expression of this gene in Matrigel culture implies either that HepG2 cells did not rely strongly on the binding of integrin subunit α5 for cellular assembly or that the fibronectin or other RGD-containing ECM proteins were not available for binding, possibly due to cleavage or decomposition, thus eliminating the needs of this gene expression [69]. Previous studies showed that HepG2-Matrigel interactions rely on α6β1 integrin [72] and that fibronectin secretion is highest during the first 24 h of spheroid formation in human dermal fibroblasts [69]. It cannot be excluded that the peak of ITGA5 may occur prior to the initial sampling point as part of initial cell aggregation. Hence, it is possible that the formation of spheroids in HepG2 cells does not critically depend on interactions between fibronectin and integrins. While fibronectin-integrin interactions may contribute to HepG2 aggregation, they may not be sufficient for spheroid formation.

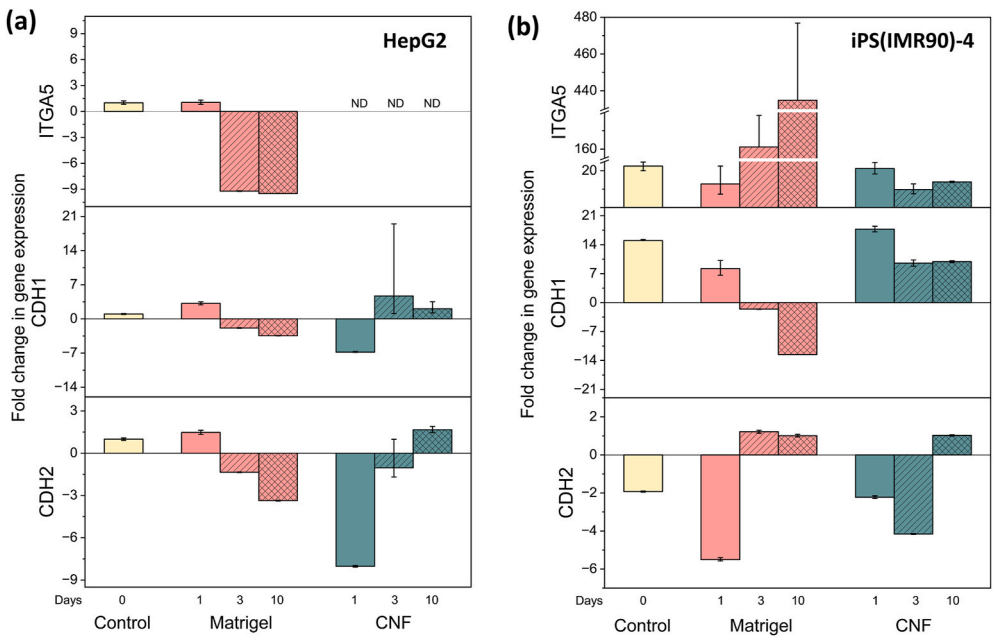

Fig. 5. *Fold change in gene expression of ITGA5, E-cadherin (CDH1) and N-cadherin (CDH2) in* ***(a)*** *HepG2 and* ***(b)*** *iPS(IMR90)-4 cells before (day 0) and after culturing in Matrigel and CNF for 1, 3, and 10 days. Fold changes and error were calculated using the ΔΔCt method [71]. Fold changes are relative to HepG2 day 0. Calibrated with TBP expression. Bars marked with ND indicate 'not detected'.*

The iPS(IMR90)-4 cells expressed ITGA5 in both hydrogel matrices. The remarkable increase in expression over time in Matrigel culture suggests that iPS(IMR90)-4 continually relied on proteins which interact with integrin subunit α5. Initial cell aggregation is a necessary condition in spheroid formation, but it does not guarantee the formation of tightly packed spheroid structure as observed from the loose clusters of iPS (IMR90)-4 in Matrigel. Therefore, the expression of CDH1 and CDH2, which encode E− and N-cadherin, was examined next.

Cadherins are important in the formation of adherens junction which mechanically connect the cytoskeleton of adjacent cells. These junctions are important for sensing and transferring mechanical stimuli between cells, maintaining cell-cell contact and facilitating collective migrations [55]. Downregulation of these cadherins indicates fewer or weaker adherens junction, promoting cell detachment from colonies and single-cell mode of migration in cancer metastasis [55].

At day 0, CDH1 expression was approximately 15-fold higher in iPS (IMR90)-4 than in HepG2. In HepG2, CDH1 and CDH2 decreased over time in Matrigel culture but increased with time in CNF culture. The decreasing cadherin expression in Matrigel culture may correspond to the looser morphology of HepG2 cells compared to CNF. In iPS(IMR90)-4, CDH1 expression decreased with time in Matrigel culture but was maintained in CNF culture after an initial decrease after day 1. CDH2 expression increased over time in both matrices. Both HepG2 and iPS (IMR90)-4 clusters remained in loose form after 48 h in Matrigel and a tight configuration developed in CNF hydrogel, which corresponds to a decreased CDH1 level in Matrigel and somewhat stable level in CNF, compared to that of day 0. This suggests that E-cadherins were involved in establishing and strengthening of cell-cell adhesion during spheroid formation. CDH2 seemed to also play a role in HepG2 spheroid formation, as can be inferred by decreased CDH2 expression in HepG2 in Matrigel cultures (where loose cell aggregates were observed) and increased in CNF cultures (where spheroids were formed). On the contrary, CDH2 is likely less important in spheroid formation in iPS (IMR90)-4 since tight spheroids were not observed for stem cells in Matrigel cultures even though the expression of CDH2 increased over time, and spheroids were formed in CNF although the expression of CDH2 was relatively low during the first days.

Given the similar viscosities of Matrigel and CNF to natural ECM proteins, it is apparent that the influencing factor on spheroid formation is the composition of the hydrogel. This implies that the different composition of each biomaterial microenvironment prompts cells to either upregulate or downregulate the expression of ECM proteins, consequently impacting the formation of spheroids as verified by gene expression.

To further our understanding of the mechanisms of spheroid formation, a detailed analysis of the distribution of measured bond ruptures events in the cell-cell and cell-material retraction force curves after 60 s of contact time was conducted (Fig. 6) and correlated to gene expression (Fig. 5). These events represent discrete force steps that signify the rupture of adhesive bonds [73]. They can manifest as jumps or tethers. In the context of bonds involving cell membrane receptors, a jump has been ascribed to the rupture of one or a few ligand-receptor bonds where the receptor remains anchored to the cell cortex, whilst a tether or membrane nanotube occurs when the receptor detaches from the cell cortex and it is pulled together with the cell membrane [25,74].

The observed event distribution displayed similarities across samples, characterised by a right-skewed distribution with a prominent single peak. However, HepG2-HepG2 exhibited a distinctive pattern with two peaks at 14 and 44 pN, that will be discussed in more detail later. Most event forces were concentrated below 100 pN, followed by a longer tail with only very few events with higher forces. Overall, Matrigel and CNF presented comparable event distributions and peak values across both cell lines. Stem cells displayed a lower amount of events/force curve with long-range forces and a significant number of events with magnitude superior to 100 pN. In contrast, HepG2 showed a higher events/force curve but most were of lower magnitude (<100 pN).

By comparing the event force distribution and the gene expression, the types of binding that occurred in early-stage cell-cell and cell-material contact were identified and the role of cadherin and integrin bonds in spheroid formation of HepG2 and iPS(IMR90)-4 was investigated. While Matrigel was expected to interact with cells via specific integrin-modulated binding – mainly via laminin-integrin α6β1 binding, inert CNF do not contain ligands for cell membrane receptors and thus, largely relies on non-specific interactions like electrostatic, hydrogen and van der Waals forces [61]. Surprisingly, the event distribution of force curves obtained from cell-material experiments of Matrigel and

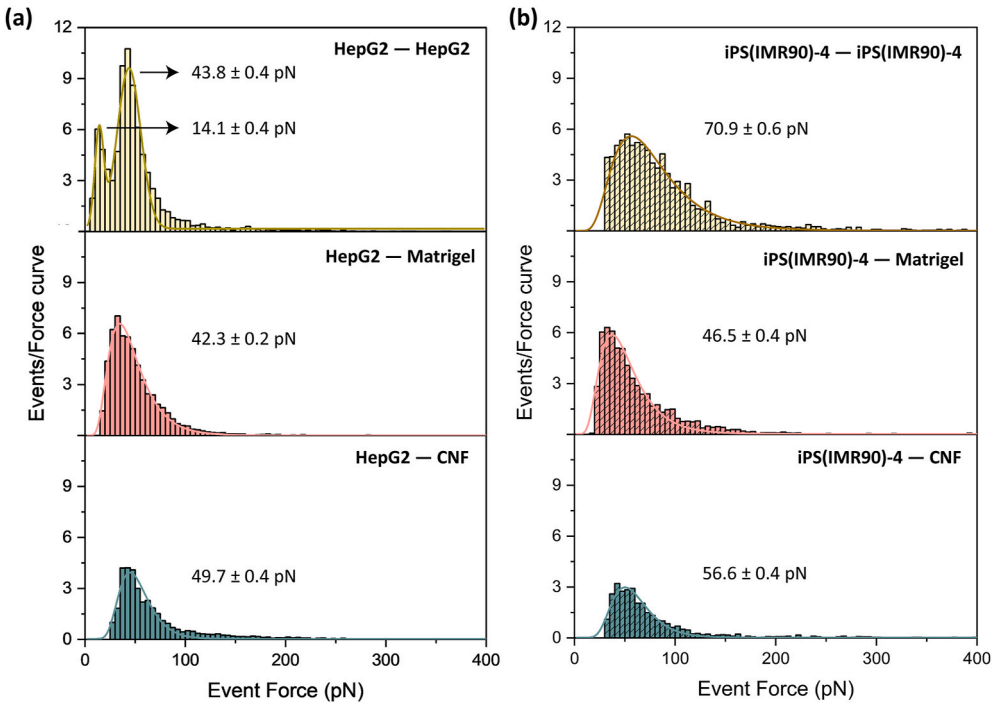

Fig. 6. Event force distribution per force curve for **(a)** HepG2 — HepG2; HepG2 — Matrigel and HepG2 — CNF and **(b)** iPS(IMR90)-4 — iPS(IMR90)-4, iPS(IMR90)-4 — Matrigel and iPS(IMR90)-4 — CNF for 60s contact time. Cell-biomaterial interactions were measured by CPM.

CNF with both cell lines displayed a single peak at rather similar forces. With Matrigel the peak was 42.3 and 46.5 pN for HepG2 and iPS (IMR90)-4, respectively, and with CNF it was 49.7 and 56.6 pN for HepG2 and iPS(IMR90)-4, respectively. The peaks in Matrigel experiments likely represent laminin-integrin α6β1 interactions as this is the most prevalent specific interaction between Matrigel and cells [68]. Although non-specific interactions like hydrogen bonds and van der Waals forces are usually considered as weak interactions, the peak recorded of cell-CNF system was slightly stronger than the peak in cell-Matrigel case. This, again, highlights the difficulties in distinguishing the effect of non-specific and specific binding.

A previous study reported force values of 48–60 pN for individual intermolecular hydrogen bond ruptures measured between COOH and NH_2 groups [75]. On the other hand, smaller forces in the range of a few pN (10–17 pN) were reported for the disruption of hydrogen bonds in DNA double helix separation [76,77]. Van de Waals forces, recognised as weak and distance-dependent interactions, were reported to be around 21–54 pN depending on the polymer and the substrate when measuring with single molecule force spectroscopy [78]. Other potential interactions in the presence of CNF could be physical entanglement of the nanofibrils with the cell membrane. This involves the stretching of cellulose fibrils until they disentangle and detach from the cell adhesion molecules. The high magnitude of the events recorded in CNF experiments suggests that the binding between CNF and cells was a result of a multitude of hydrogen bonds or van der Waals attractions. Despite being non-specific interactions, they can result in strong adhesion forces and energy even higher than specific binding. However, it is worth noting that the experiments involved the application of a certain force of the cells to CNF substrate. Therefore, the recorded value might overestimate the true CNF-cell interaction.

The event force distribution for HepG2-HepG2 revealed two distinct peaks (Fig. 6), at 14 and 44 pN. Since the peak at 44 pN is at a similar magnitude with the peak found in the cell-Matrigel system, it is possible that it also represents an integrin-modulated adhesion, which is likely to be integrin subunit α5 binding to RGD-featured proteins, in line with the expression of ITGA5 of HepG2 on day 0. As the ITGA5 expression level of iPS(IMR90-4) was much higher compared to HepG2, it was expected that a peak at similar range (~40–50 pN) would appear in the event force distribution for iPS(IMR90)-4. However, a single broad peak was observed in the cell-cell experiments for iPS(IMR90)-4 instead, spanning from 40 to 90 pN. We speculate that the ECM protein-integrin α5 also occurred, but the representative peak for this interaction overlapped with another stronger adhesion between iPS(IMR90)-4 cells. Since the iPS(IMR90)-4 expressed higher levels of CDH1 on day 0, potentially corresponding to a higher level of E-cadherins availability, compared to HepG2, we believe that this stronger adhesion may represent the establishment and breaking of E-cadherin homophilic bonds between stem cells.

A small peak at 14.1 pN was also observed from the HepG2-HepG2 experiments. This peak likely represents N-cadherin-N-cadherin binding. This is supported by the fact that HepG2 had higher CDH2 expression on day 0 (which suggests a higher level of N-cadherins expressed) compared to iPS(IMR90)-4. In agreement with this, the corresponding peak was absent from the event distribution of the stem cells. These values agree with reports for N-cadherin bonds which range from 17 to 40 pN [79,80] and values for E-cadherin which range from 73 to 157 pN [79]. The specific cadherins involved in spheroid compaction varies between cell types [81,82]. E-cadherin participates in tight packing in renal cell carcinoma cell lines and in MCF7, BT-474, T-47D and MDA-MB-361 breast cancer cell lines, whereas N-cadherin was responsible for spheroid formation in MDA-MB-435S cells [83,84]. Cadherin-independent spheroid formation, instead relying on integrin β-collagen I interaction had also been reported [85]. Our results suggest that E- and N-cadherins are implicated in the tight binding of HepG2 and iPS(IMR90)-4 cells to form compact spheroids.

As Matrigel largely interacted with both cell lines via laminin-integrin α6β1 binding and CDH1 gene (encoding E-cadherins) was downregulated in both cell lines, we hypothesize that the formation of integrin-laminin bonds or a component of Matrigel may downregulate the expression of E-cadherins, hindering the compaction of spheroid culture. E-cadherins are suspected to play important role in facilitating and tightening cell-cell adhesions for both cell lines.

The initial hypothesis was that if cell-material interactions were stronger than cell-cell interactions, spheroid formation would be

disrupted and vice versa. However, the results of both cell cultures and AFM force measurements suggest that total adhesion force and adhesion energy are not the decisive factors as they result from the combination of several types of bonds (specific or non-specific, depending on the system) with binding forces in a similar range of tens of pN. The types of dominant specific bonds established in early as well as in later stage (i.e., integrin and cadherin-based bonds, and which specific cellular receptors are involved) play a more significant role in deciding the outcome of the spheroid culture, rather than the total amount of bonds encompassed in the adhesion energy.

Based on the results, we hypothesize that firstly, at early stage upon contact, both HepG2 and iPS(IMR90)-4 relied on ECM protein-integrin binding, specifically α5 integrin subunit, to establish initial cellular assembly. The lack of α5 expression might be the reason of insufficient volume of cell aggregates, as observed in the case of HepG2 embedded in CNF. Secondly, although the two studied cell lines have their own preferential cadherin species to form cell-cell tight binding, HepG2 favouring N-cadherins and iPS(IMR90)-4 employing E-cadherins, cadherins play a crucial role in the evolution of loose cell aggregates into tight spheroids for both cell lines. Matrigel can establish specific interactions with both cell lines via laminin-integrin α6β1 binding. However, a decrease in CDH1 gene expression led us to suspect that this Matrigel binding or a component in Matrigel has caused a down-regulation of E-cadherins, which led to cell clusters remaining in loose configuration. Conversely, the conditions in CNF hydrogel could promote CDH1 expression in both lines. Despite the lack of specific interactions with CNF, both cell lines cultured in CNF hydrogels saw a rapid formation of a population of compact cell clusters or spheroids. This reveals that the complexity of adhesion proteins and biomaterials directly affects cell behaviour, contributing to our broader understanding of cellular interactions in different environments.

4. Conclusion

In this study, the complex mechanisms governing cell-biomaterial interactions and their implications for spheroid formation were explored. Using AFM-based techniques, the adhesion forces of HepG2 and iPS(IMR90)-4 cells to Matrigel, CNF hydrogels, as well as cell-cell adhesion were quantified. Combined with cell culture experiments and qRT-PCR, insights into the effects of cell-cell and cell-material interactions on spheroid formation were gained. The cell culture and gene expression results showed distinct behaviours in the two cell lines when cultured in CNF and Matrigel. Within 72 h, both cell lines formed compact spheroids in CNF hydrogel, indicating a favourable environment for cell-cell interactions. In contrast, Matrigel cultures led to the formation of large loose cell aggregates, that did not condense into tightly packed spheroids.

In addition, it was shown that this distinct behaviour was not explained by adhesion forces and energy values alone. Further analysis of AFM force curves and qRT-PCR data revealed important adhesion types at the early stages of cell-cell and cell-material contact and their contribution to spheroid formation. Both cell lines relied on ECM protein-integrin binding, particularly the binding between integrin subunit α5 and RGD-containing proteins, for initial cellular assembly or aggregation. Although E-cadherin expression appeared essential for spheroid compaction in both HepG2 and iPS(IMR90)-4, each cell line interacted using different cadherin species during the early stages of spheroid formation. Stem cells relied mainly on E-cadherins, while HepG2 cells relied on N-cadherins. However, integrin-laminin interactions in Matrigel or a component of that matrix seemed to down-regulate the expression of E-cadherins over time, impeding spheroid compaction.

Our findings suggest that detailed analysis of cell interactions using AFM in combination with cell culture and gene expression is a powerful toolset to understand cell behaviour. These results showed that the types of interactions and ligands or receptors involved, as well as the strength and number of binding sites, influenced cell adhesion and the resulting cellular assembly. This study provides insights into the distinct dependencies on adhesion proteins and the resulting cellular behaviours in different biomaterial environments, based on empirical and quantitative data. These findings furthermore advance our understanding on spheroid formation and the effects of environment, contributing to the development of *in vitro* spheroid models and thereby reducing the need for animal testing.

CRediT authorship contribution statement

Roberta Teixeira Polez: Writing – original draft, Visualization, Validation, Methodology, Investigation, Formal analysis, Data curation. **Ngoc Huynh:** Writing – original draft, Visualization, Validation, Methodology, Investigation, Formal analysis, Data curation, Conceptualization. **Chris S. Pridgeon:** Writing – review & editing, Methodology, Investigation, Formal analysis. **Juan José Valle-Delgado:** Writing – review & editing, Supervision, Investigation, Formal analysis. **Riina Harjumäki:** Writing – review & editing, Resources, Investigation, Funding acquisition, Formal analysis, Conceptualization. **Monika Österberg:** Writing – review & editing, Supervision, Resources, Investigation, Funding acquisition.

Declaration of competing interest

The authors declare that they have no known competing financial interests or personal relationships that could have appeared to influence the work reported in this paper.

Data availability

Data will be made available on request.

Acknowledgments

This work was a part of the Academy of Finland's Flagship Program (project numbers 318890 and 318891, Competence Center for Materials Bioeconomy, FinnCERES). This work was also funded with grants Academy of Finland, GeneCellNano flagship-project (grant no. 337430), Finnish Cultural Foundation (grant no. 00220283) and Jenny and Antti Wihuri Foundation. The authors would like to acknowledge the Finnish-American Research and Innovation Accelerator funding (project number 9758124), and Drug Discovery and Chemical Biology Network (funded by Biocenter Finland) for providing access to Varioskan. The authors would also like to thank Thales de Oliveira Gonçalves, Tran Nguyen Le and James M. Rocker for creating the Python code. This work made use of Aalto University Bioeconomy Facilities. Imaging was performed at the Light Microscopy Unit, Institute of Biotechnology, supported by HiLIFE and Biocenter Finland.

Appendix A. Supplementary data

Supplementary data to this article can be found online at https://doi.org/10.1016/j.mtbio.2024.101065.

References

[1] F. Pampaloni, E.G. Reynaud, E.H.K. Stelzer, The third dimension bridges the gap between cell culture and live tissue, Nat. Rev. Mol. Cell Biol. 8 (2007) 839–845, https://doi.org/10.1038/nrm2236.

[2] N.-H. Lee, O. Bayaraa, Z. Zechu, H.S. Kim, Biomaterials-assisted spheroid engineering for regenerative therapy, BMB Rep 54 (2021) 356–367, https://doi.org/10.5483/BMBRep.2021.54.7.059.

[3] S.H. Kwon, S.H. Bhang, H.-K. Jang, T. Rhim, B.-S. Kim, Conditioned medium of adipose-derived stromal cell culture in three-dimensional bioreactors for enhanced wound healing, J. Surg. Res. 194 (2015) 8–17, https://doi.org/10.1016/j.jss.2014.10.053.

[4] C.S. Ong, X. Zhou, J. Han, C.Y. Huang, A. Nashed, S. Khatri, G. Mattson, T. Fukunishi, H. Zhang, N. Hibino, In vivo therapeutic applications of cell spheroids, Biotechnol. Adv. 36 (2018) 494–505, https://doi.org/10.1016/j.biotechadv.2018.02.003.

[5] R. Nuwer, US agency seeks to phase out animal testing, Nature (2022), https://doi.org/10.1038/d41586-022-03569-9.

[6] M. Wadman, FDA no longer has to require animal testing for new drugs, Science (2023), https://doi.org/10.1126/science.adg6276.

[7] S. Kim, E.M. Kim, M. Yamamoto, H. Park, H. Shin, Engineering multi-cellular spheroids for tissue engineering and regenerative medicine, Adv Healthc Mater 9 (2020) 2000608, https://doi.org/10.1002/adhm.202000608.

[8] J. Ko, J. Park, J. Kim, G. Im, Characterization of adipose-derived stromal/stem cell spheroids versus single-cell suspension in cell survival and arrest of osteoarthritis progression, J. Biomed. Mater. Res. 109 (2021) 869–878, https://doi.org/10.1002/jbm.a.37078.

[9] C.S. Hughes, L.M. Postovit, G.A. Lajoie, Matrigel: a complex protein mixture required for optimal growth of cell culture, Proteomics 10 (2010) 1886–1890, https://doi.org/10.1002/pmic.200900758.

[10] Y. Fang, R.M. Eglen, Three-dimensional cell cultures in drug discovery and development, SLAS Discovery 22 (2017) 456–472, https://doi.org/10.1177/1087057117696795.

[11] B.A. Justice, N.A. Badr, R.A. Felder, 3D cell culture opens new dimensions in cell-based assays, Drug Discov. Today 14 (2009) 102–107, https://doi.org/10.1016/j.drudis.2008.11.006.

[12] R.T. Polez, M. Morits, C. Jonkergouw, J. Phiri, J.J. Valle-Delgado, M.B. Linder, T. Maloney, O.J. Rojas, M. Österberg, Biological activity of multicomponent bio-hydrogels loaded with tragacanth gum, Int. J. Biol. Macromol. 215 (2022) 691–704, https://doi.org/10.1016/j.ijbiomac.2022.06.153.

[13] H. Baniasadi, E. Kimiaei, R.T. Polez, R. Ajdary, O.J. Rojas, M. Österberg, J. Seppälä, High-resolution 3D printing of xanthan gum/nanocellulose bio-inks, Int. J. Biol. Macromol. 209 (2022) 2020–2031, https://doi.org/10.1016/j.ijbiomac.2022.04.183.

[14] H. Baniasadi, R.T. Polez, E. Kimiaei, Z. Madani, O.J. Rojas, M. Österberg, J. Seppälä, 3D printing and properties of cellulose nanofibrils-reinforced quince seed mucilage bio-inks, Int. J. Biol. Macromol. 192 (2021) 1098–1107, https://doi.org/10.1016/j.ijbiomac.2021.10.078.

[15] R. Koivuniemi, Q. Xu, J. Snirvi, I. Lara-Sáez, A. Merivaara, K. Luukko, M. Nuopponen, W. Wang, M. Yliperttula, Comparison of the therapeutic effects of native and anionic nanofibrillar cellulose hydrogels for full-thickness skin wound healing, Micro 1 (2021) 194–214, https://doi.org/10.3390/micro1020015.

[16] J. Kiiskinen, A. Merivaara, T. Hakkarainen, M. Kääriäinen, S. Miettinen, M. Yliperttula, R. Koivuniemi, Nanofibrillar cellulose wound dressing supports the growth and characteristics of human mesenchymal stem/stromal cells without cell adhesion coatings, Stem Cell Res. Ther. 10 (2019) 292, https://doi.org/10.1186/s13287-019-1394-7.

[17] R. Koivuniemi, T. Hakkarainen, J. Kiiskinen, M. Kosonen, J. Vuola, J. Valtonen, K. Luukko, H. Kavola, M. Yliperttula, Clinical study of nanofibrillar cellulose hydrogel dressing for skin graft donor site treatment, Adv. Wound Care 9 (2020) 199–210, https://doi.org/10.1089/wound.2019.0982.

[18] M.M. Malinen, L.K. Kanninen, A. Corlu, H.M. Isoniemi, Y.-R. Lou, M.L. Yliperttula, A.O. Urtti, Differentiation of liver progenitor cell line to functional organotypic cultures in 3D nanofibrillar cellulose and hyaluronan-gelatin hydrogels, Biomaterials 35 (2014) 5110–5121, https://doi.org/10.1016/j.biomaterials.2014.03.020.

[19] Y. Nie, X. Xu, W. Wang, N. Ma, A. Lendlein, Spheroid formation of human keratinocyte: balancing between cell-substrate and cell-cell interaction, Clin. Hemorheol. Microcirc. 76 (2020) 329–340, https://doi.org/10.3233/CH-209217.

[20] M.S. Bogacheva, R. Harjumäki, E. Flander, A. Taalas, M.A. Bystriakova, M. Yliperttula, X. Xiang, A.W. Leung, Y.-R. Lou, Differentiation of human pluripotent stem cells into definitive endoderm cells in various flexible three-dimensional cell culture systems: possibilities and limitations, Front. Cell Dev. Biol. 9 (2021) 726499, https://doi.org/10.3389/fcell.2021.726499.

[21] C. Xu, M.S. Inokuma, J. Denham, K. Golds, P. Kundu, J.D. Gold, M.K. Carpenter, Feeder-free growth of undifferentiated human embryonic stem cells, Nat. Biotechnol. 19 (2001) 971–974, https://doi.org/10.1038/nbt1001-971.

[22] M. Bhattacharya, M.M. Malinen, P. Lauren, Y.-R. Lou, S.W. Kuisma, L. Kanninen, M. Lille, A. Corlu, C. GuGuen-Guillouzo, O. Ikkala, A. Laukkanen, A. Urtti, M. Yliperttula, Nanofibrillar cellulose hydrogel promotes three-dimensional liver cell culture, J. Contr. Release 164 (2012) 291–298, https://doi.org/10.1016/j.jconrel.2012.06.039.

[23] Y.-R. Lou, L. Kanninen, T. Kuisma, J. Niklander, L.A. Noon, D. Burks, A. Urtti, M. Yliperttula, The use of nanofibrillar cellulose hydrogel as a flexible three-dimensional model to culture human pluripotent stem cells, Stem Cells Dev 23 (2014) 380–392, https://doi.org/10.1089/scd.2013.0314.

[24] R. Harjumäki, R.W.N. Nugroho, X. Zhang, Y.-R. Lou, M. Yliperttula, J.J. Valle-Delgado, M. Österberg, Quantified forces between HepG2 hepatocarcinoma and WA07 pluripotent stem cells with natural biomaterials correlate with in vitro cell behavior, Sci. Rep. 9 (2019) 7354, https://doi.org/10.1038/s41598-019-43669-7.

[25] A.V. Taubenberger, D.W. Hutmacher, D.J. Muller, Single-cell force spectroscopy, an emerging tool to quantify cell adhesion to biomaterials, Tissue Eng Part B Rev 20 (2014) 40–55, https://doi.org/10.1089/ten.teb.2013.0125.

[26] J. Schindelin, I. Arganda-Carreras, E. Frise, V. Kaynig, M. Longair, T. Pietzsch, S. Preibisch, C. Rueden, S. Saalfeld, B. Schmid, J.-Y. Tinevez, D.J. White, V. Hartenstein, K. Eliceiri, P. Tomancak, A. Cardona, Fiji: an open-source platform for biological-image analysis, Nat. Methods 9 (2012) 676–682, https://doi.org/10.1038/nmeth.2019.

[27] R.W.N. Nugroho, R. Harjumäki, X. Zhang, Y.-R. Lou, M. Yliperttula, J.J. Valle-Delgado, M. Österberg, Quantifying the interactions between biomimetic biomaterials – collagen I, collagen IV, laminin 521 and cellulose nanofibrils – by colloidal probe microscopy, Colloids Surf. B Biointerfaces 173 (2019) 571–580, https://doi.org/10.1016/j.colsurfb.2018.09.073.

[28] J.J. Valle-Delgado, L.-S. Johansson, M. Österberg, Bioinspired lubricating films of cellulose nanofibrils and hyaluronic acid, Colloids Surf. B Biointerfaces 138 (2016) 86–93, https://doi.org/10.1016/j.colsurfb.2015.11.047.

[29] J. Friedrichs, J. Helenius, D.J. Muller, Quantifying cellular adhesion to extracellular matrix components by single-cell force spectroscopy, Nat. Protoc. 5 (2010) 1353–1361, https://doi.org/10.1038/nprot.2010.89.

[30] C.A. Schneider, W.S. Rasband, K.W. Eliceiri, NIH Image to ImageJ: 25 years of image analysis, Nat. Methods 9 (2012) 671–675, https://doi.org/10.1038/nmeth.2089.

[31] J.L. Hutter, J. Bechhoefer, Calibration of atomic-force microscope tips, Rev. Sci. Instrum. 64 (1993) 1868–1873, https://doi.org/10.1063/1.1143970.

[32] J. Laurent, A. Steinberger, L. Bellon, Functionalized AFM probes for force spectroscopy: eigenmode shapes and stiffness calibration through thermal noise measurements, Nanotechnology 24 (2013) 225504, https://doi.org/10.1088/0957-4484/24/22/225504.

[33] R. Edmondson, J.J. Broglie, A.F. Adcock, L. Yang, Three-dimensional cell culture systems and their applications in drug Discovery and cell-based biosensors, Assay Drug Dev. Technol. 12 (2014) 207–218, https://doi.org/10.1089/adt.2014.573.

[34] E. Koivunotko, J. Snirvi, A. Merivaara, R. Harjumäki, S. Rautiainen, M. Kelloniemi, K. Kuismanen, S. Miettinen, M. Yliperttula, R. Koivuniemi, Angiogenic potential of human adipose-derived mesenchymal stromal cells in nanofibrillated cellulose hydrogel, Biomedicines 10 (2022) 2584, https://doi.org/10.3390/biomedicines10102584.

[35] M. Huch, H. Gehart, R. van Boxtel, K. Hamer, F. Blokzijl, M.M.A. Verstegen, E. Ellis, M. van Wenum, S.A. Fuchs, J. de Ligt, M. van de Wetering, N. Sasaki, S. J. Boers, H. Kemperman, J. de Jonge, J.N.M. Ijzermans, E.E.S. Nieuwenhuis, R. Hoekstra, S. Strom, R.R.G. Vries, L.J.W. van der Laan, E. Cuppen, H. Clevers, Long-term culture of genome-stable bipotent stem cells from adult human liver, Cell 160 (2015) 299–312, https://doi.org/10.1016/j.cell.2014.11.050.

[36] M.A. Badea, M. Balas, A. Hermenean, A. Ciceu, H. Herman, D. Ionita, A. Dinischiotu, Influence of Matrigel on single- and multiple-spheroid cultures in breast cancer research, SLAS Discovery 24 (2019) 563–578, https://doi.org/10.1177/2472555219834698.

[37] K.M. Tevis, Y.L. Colson, M.W. Grinstaff, Embedded spheroids as models of the cancer microenvironment, Adv Biosyst 1 (2017) 1700083, https://doi.org/10.1002/adbi.201700083.

[38] R.-Z. Lin, L.-F. Chou, C.-C.M. Chien, H.-Y. Chang, Dynamic analysis of hepatoma spheroid formation: roles of E-cadherin and β1-integrin, Cell Tissue Res. 324 (2006) 411–422, https://doi.org/10.1007/s00441-005-0148-2.

[39] N.E. Ryu, S.H. Lee, H. Park, Spheroid culture system methods and applications for mesenchymal stem cells, Cells 8 (2019) 1620, https://doi.org/10.3390/cells8121620.

[40] D. Janzen, E. Bakirci, A. Wieland, C. Martin, P.D. Dalton, C. Villmann, Cortical neurons form a functional neuronal network in a 3D printed reinforced matrix, Adv Healthc Mater 9 (2020) 1901630, https://doi.org/10.1002/adhm.201901630.

[41] D.A. Young, D.O. Ibrahim, D. Hu, K.L. Christman, Injectable hydrogel scaffold from decellularized human lipoaspirate, Acta Biomater. 7 (2011) 1040–1049, https://doi.org/10.1016/j.actbio.2010.09.035.

[42] R.A. Pouliot, P.A. Link, N.S. Mikhaiel, M.B. Schneck, M.S. Valentine, F.J. Kamga Gninzeko, J.A. Herbert, M. Sakagami, R.L. Heise, Development and characterization of a naturally derived lung extracellular matrix hydrogel, J. Biomed. Mater. Res. 104 (2016) 1922–1935, https://doi.org/10.1002/jbm.a.35726.

[43] A. Merivaara, E. Koivunotko, K. Manninen, T. Kaseva, J. Monola, E. Salli, R. Koivuniemi, S. Savolainen, S. Valkonen, M. Yliperttula, Stiffness-controlled hydrogels for 3D cell culture models, Polymers 14 (2022) 5530, https://doi.org/10.3390/polym14245530.

[44] Y.-R. Lou, L. Kanninen, B. Kaehr, J.L. Townson, J. Niklander, R. Harjumäki, C. Jeffrey Brinker, M. Yliperttula, Silica bioreplication preserves three-dimensional spheroid structures of human pluripotent stem cells and HepG2 cells, Sci. Rep. 5 (2015) 13635, https://doi.org/10.1038/srep13635.

[45] S.-Y. Lee, Y. Teng, M. Son, B. Ku, H.J. Hwang, V. Tergaonkar, P.K.-H. Chow, D. W. Lee, D.-H. Nam, Three-dimensional aggregated spheroid model of hepatocellular carcinoma using a 96-pillar/well plate, Molecules 26 (2021) 4949, https://doi.org/10.3390/molecules26164949.

[46] S.C. Ramaiahgari, M.W. den Braver, B. Herpers, V. Terpstra, J.N.M. Commandeur, B. van de Water, L.S. Price, A 3D in vitro model of differentiated HepG2 cell spheroids with improved liver-like properties for repeated dose high-throughput toxicity studies, Arch. Toxicol. 88 (2014) 1083–1095, https://doi.org/10.1007/s00204-014-1215-9.

[47] C. Luckert, C. Schulz, N. Lehmann, M. Thomas, U. Hofmann, S. Hammad, J. G. Hengstler, A. Braeuning, A. Lampen, S. Hessel, Comparative analysis of 3D culture methods on human HepG2 cells, Arch. Toxicol. 91 (2017) 393–406, https://doi.org/10.1007/s00204-016-1677-z.

[48] K.J. Lynch, O. Skalli, F. Sabri, Investigation of surface topography and stiffness on adhesion and neurites extension of PC12 cells on crosslinked silica aerogel substrates, PLoS One 12 (2017) e0185978, https://doi.org/10.1371/journal.pone.0185978.

[49] H. Mao, Y. Ito, Engineering niches for embryonic and induced pluripotent stem cells, in: Biology and Engineering of Stem Cell Niches, Academic Press, 2017, pp. 445–457, https://doi.org/10.1016/B978-0-12-802734-9.00028-7.

[50] H. Holuigue, L. Nacci, P. Di Chiaro, M. Chighizola, I. Locatelli, C. Schulte, M. Alfano, G.R. Diaferia, A. Podestà, Novel native extracellular matrix probes to target patient- and tissue- specific cell-microenvironment interactions by force spectroscopy, bioRxiv (2022), https://doi.org/10.1101/2022.12.02.518867.
[51] R. Harjumäki, X. Zhang, R.W.N. Nugroho, M. Farooq, Y. Lou, M. Yliperttula, J. J. Valle-Delgado, M. Österberg, AFM force spectroscopy reveals the role of integrins and their activation in cell–biomaterial interactions, ACS Appl. Bio Mater. 3 (2020) 1406–1417, https://doi.org/10.1021/acsabm.9b01073.
[52] L. Dao, U. Weiland, M. Hauser, I. Nazarenko, H. Kalt, M. Bastmeyer, C.M. Franz, Revealing non-genetic adhesive variations in clonal populations by comparative single-cell force spectroscopy, Exp. Cell Res. 318 (2012) 2155–2167, https://doi.org/10.1016/j.yexcr.2012.06.017.
[53] M. Sztilkovics, T. Gerecsei, B. Peter, A. Saftics, S. Kurunczi, I. Szekacs, B. Szabo, R. Horvath, Single-cell adhesion force kinetics of cell populations from combined label-free optical biosensor and robotic fluidic force microscopy, Sci. Rep. 10 (2020) 61, https://doi.org/10.1038/s41598-019-56898-7.
[54] J. Friedrichs, K.R. Legate, R. Schubert, M. Bharadwaj, C. Werner, D.J. Müller, M. Benoit, A practical guide to quantify cell adhesion using single-cell force spectroscopy, Methods 60 (2013) 169–178, https://doi.org/10.1016/j.ymeth.2013.01.006.
[55] E. Barcelona-Estaje, M.J. Dalby, M. Cantini, M. Salmeron-Sanchez, You talking to me? Cadherin and integrin crosstalk in biomaterial design, Adv Healthc Mater 10 (2021) 2002048, https://doi.org/10.1002/adhm.202002048.
[56] S. Schumacher, D. Dedden, R.V. Nunez, K. Matoba, J. Takagi, C. Biertümpfel, N. Mizuno, Structural insights into integrin α5β1 opening by fibronectin ligand, Sci. Adv. 7 (2021) eabe9716, https://doi.org/10.1126/sciadv.abe9716.
[57] T. Arimori, N. Miyazaki, E. Mihara, M. Takizawa, Y. Taniguchi, C. Cabañas, K. Sekiguchi, J. Takagi, Structural mechanism of laminin recognition by integrin, Nat. Commun. 12 (2021) 4012, https://doi.org/10.1038/s41467-021-24184-8.
[58] Y. Meng, S. Eshghi, Y.J. Li, R. Schmidt, D.V. Schaffer, K.E. Healy, Characterization of integrin engagement during defined human embryonic stem cell culture, Faseb. J. 24 (2010) 1056–1065, https://doi.org/10.1096/fj.08-126821.
[59] F. Pincet, T. Le Bouar, Y. Zhang, J. Esnault, J.-M. Mallet, E. Perez, P. Sinaÿ, Ultraweak sugar-sugar interactions for transient cell adhesion, Biophys. J. 80 (2001) 1354–1358, https://doi.org/10.1016/S0006-3495(01)76108-5.
[60] X. Zhang, T. Viitala, R. Harjumäki, A. Kartal-Hodzic, J.J. Valle-Delgado, M. Österberg, Effect of laminin, polylysine and cell medium components on the attachment of human hepatocellular carcinoma cells to cellulose nanofibrils analyzed by surface plasmon resonance, J. Colloid Interface Sci. 584 (2021) 310–319, https://doi.org/10.1016/j.jcis.2020.09.080.
[61] A.A. Gurtovenko, E.I. Mukhamadiarov, A.Yu Kostritskii, M. Karttunen, Phospholipid–cellulose interactions: insight from atomistic computer simulations for understanding the impact of cellulose-based materials on plasma membranes, J. Phys. Chem. B 122 (2018) 9973–9981, https://doi.org/10.1021/acs.jpcb.8b07765.
[62] E. Dalir Abdolahinia, B. Jafari, S. Parvizpour, J. Barar, S. Nadri, Y. Omidi, Role of cellulose family in fibril organization of collagen for forming 3D cancer spheroids: in vitro and in silico approach, Bioimpacts 11 (2020) 111–117, https://doi.org/10.34172/bi.2021.18.
[63] K. Pogoda, R. Bucki, F.J. Byfield, K. Cruz, T. Lee, C. Marcinkiewicz, P.A. Janmey, Soft substrates containing hyaluronan mimic the effects of increased stiffness on morphology, motility, and proliferation of glioma cells, Biomacromolecules 18 (2017) 3040–3051, https://doi.org/10.1021/acs.biomac.7b00324.
[64] J.W. Weisel, H. Shuman, R.I. Litvinov, Protein–protein unbinding induced by force: single-molecule studies, Curr. Opin. Struct. Biol. 13 (2003) 227–235, https://doi.org/10.1016/S0959-440X(03)00039-3.
[65] P.S. Raman, C.S. Alves, D. Wirtz, K. Konstantopoulos, Distinct kinetic and molecular requirements govern CD44 binding to hyaluronan versus fibrin(ogen), Biophys. J. 103 (2012) 415–423, https://doi.org/10.1016/j.bpj.2012.06.039.
[66] X. Cui, Y. Hartanto, C. Wu, J. Bi, S. Dai, H. Zhang, Tuning microenvironment for multicellular spheroid formation in thermo-responsive anionic microgel scaffolds, J. Biomed. Mater. Res. 106 (2018) 2899–2909, https://doi.org/10.1002/jbm.a.36479.
[67] E. Ruoslahti, Integrins, J. Clin. Invest. 87 (1991) 1–5, https://doi.org/10.1172/JCI114957.
[68] T.J. Rowland, L.M. Miller, A.J. Blaschke, E.L. Doss, A.J. Bonham, S.T. Hikita, L. V. Johnson, D.O. Clegg, Roles of integrins in human induced pluripotent stem cell growth on Matrigel and vitronectin, Stem Cells Dev 19 (2010) 1231–1240, https://doi.org/10.1089/scd.2009.0328.
[69] P. Salmenperä, E. Kankuri, J. Bizik, V. Sirén, I. Virtanen, S. Takahashi, M. Leiss, R. Fässler, A. Vaheri, Formation and activation of fibroblast spheroids depend on fibronectin–integrin interaction, Exp. Cell Res. 314 (2008) 3444–3452, https://doi.org/10.1016/j.yexcr.2008.09.004.
[70] S. Chae, J. Hong, H. Hwangbo, G. Kim, The utility of biomedical scaffolds laden with spheroids in various tissue engineering applications, Theranostics 11 (2021) 6818–6832, https://doi.org/10.7150/thno.58421.
[71] K.J. Livak, T.D. Schmittgen, Analysis of relative gene expression data using real-time quantitative PCR and the 2−ΔΔCT method, Methods 25 (2001) 402–408, https://doi.org/10.1006/meth.2001.1262.
[72] V. Carloni, R.G. Romanelli, A.M. Mercurio, M. Pinzani, G. Laffi, G. Cotrozzi, P. Gentilini, Knockout of α6β1-integrin expression reverses the transformed phenotype of hepatocarcinoma cells, Gastroenterology 115 (1998) 433–442, https://doi.org/10.1016/S0016-5085(98)70210-0.
[73] J. Helenius, C.-P. Heisenberg, H.E. Gaub, D.J. Muller, Single-cell force spectroscopy, J. Cell Sci. 121 (2008) 1785–1791, https://doi.org/10.1242/jcs.030999.
[74] D.J. Müller, J. Helenius, D. Alsteens, Y.F. Dufrêne, Force probing surfaces of living cells to molecular resolution, Nat. Chem. Biol. 5 (2009) 383–390, https://doi.org/10.1038/nchembio.181.
[75] S. Kado, T. Murakami, K. Kimura, Effect of intramonolayer hydrogen bonding of carboxyl groups in self-assembled monolayers on a single force with phenylurea on an AFM probe tip, Anal. Sci. 22 (2006) 521–527, https://doi.org/10.2116/analsci.22.521.
[76] B. Essevaz-Roulet, U. Bockelmann, F. Heslot, Mechanical separation of the complementary strands of DNA, Proc. Natl. Acad. Sci. USA 94 (1997) 11935–11940, https://doi.org/10.1073/pnas.94.22.11935.
[77] T. Naranjo, F. Cerrón, B. Nieto-Ortega, A. Latorre, Á. Somoza, B. Ibarra, E.M. Pérez, Mechanical measurement of hydrogen bonded host–guest systems under non-equilibrium, near-physiological conditions, Chem. Sci. 8 (2017) 6037–6041, https://doi.org/10.1039/C7SC03044D.
[78] W. Cai, C. Xiao, L. Qian, S. Cui, Detecting van der Waals forces between a single polymer repeating unit and a solid surface in high vacuum, Nano Res. 12 (2019) 57–61, https://doi.org/10.1007/s12274-018-2176-8.
[79] P. Panorchan, M.S. Thompson, K.J. Davis, Y. Tseng, K. Konstantopoulos, D. Wirtz, Single-molecule analysis of cadherin-mediated cell-cell adhesion, J. Cell Sci. 119 (2006) 66–74, https://doi.org/10.1242/jcs.02719.
[80] P. Panorchan, J.P. George, D. Wirtz, Probing intercellular interactions between vascular endothelial cadherin pairs at single-molecule resolution and in living cells, J. Mol. Biol. 358 (2006) 665–674, https://doi.org/10.1016/j.jmb.2006.02.021.
[81] R. Goel, D. Gulwani, P. Upadhyay, V. Sarangthem, T.D. Singh, Unsung versatility of elastin-like polypeptide inspired spheroid fabrication: a review, Int. J. Biol. Macromol. 234 (2023) 123664, https://doi.org/10.1016/j.ijbiomac.2023.123664.
[82] X. Cui, Y. Hartanto, H. Zhang, Advances in multicellular spheroids formation, J R Soc Interface 14 (2017) 20160877, https://doi.org/10.1098/rsif.2016.0877.
[83] T. Shimazui, J. Schalken, K. Kawai, R. Kawamoto, A. Van Bockhoven, E. Oosterwijk, H. Akaza, Role of complex cadherins in cell-cell adhesion evaluated by spheroid formation in renal cell carcinoma cell lines, Oncol. Rep. 11 (2004) 357–360, https://doi.org/10.3892/or.11.2.357.
[84] A. Ivascu, M. Kubbies, Diversity of cell-mediated adhesions in breast cancer spheroids, Int. J. Oncol. 31 (2007) 1403–1413, https://doi.org/10.3892/ijo.31.6.1403.
[85] A. Ivascu, M. Kubbies, Rapid generation of single-tumor spheroids for high-throughput cell function and toxicity analysis, SLAS Discovery 11 (2006) 922–932, https://doi.org/10.1177/1087057106292763.